A Comparison of Subnetwork Classification Methods

Elizabeth Powell, Ferran Prados, Wallace Brownlee, Baris Kanber, Sara Collorone, Sebastien Ourselin, Olga Ciccarelli, Ahmed Toosy, Jonathan D Clayden, Claudia A Gandini Wheeler-Kingshott.

Introduction: In the complex network model of the human brain, it is often noted that a subset of nodes play a central role in network architecture[refs]. Hub nodes, for example, exhibit high degree properties, and are thus important for network integration; however, local damage to hub nodes may have a disproportionate effect on network resilience to injury.

The "rich club" phenomenon[ref] proposes a description in which hub nodes are densely interconnected with fewer connections to lower degree nodes. The regions that form these rich clubs can be classified as a subnetwork, offering high communication efficiency and some level of network resilience to the failure of a hub node.

The identification of "important" nodes in a network is non-trivial though, and there exist alternative methods of extracting salient regions. Recently, the concept of principal networks[ref] was introduced. Principal network analysis (PNA) involves the eigendecomposition of the association matrix, $\mathbf{A}$, into its canonical form ($A = Q\Lambda Q^{-1}$). The eigenvector element Q_{ij}, or loading, represents the influence of node i on principal network (PN) j. PNs are subsequently formed from nodes with similar connectivity properties.

In this work we examine the agreement between two independent techniques, namely rich club analysis and PNA, used for extracting subnetworks based on key nodes from cortical thickness data.

Methods: T_1-weighted images were acquired on 46 healthy controls (26 females; mean age 34 ± 8.6 years); imaging parameters and hardware specifications are given in Figure 1. The thickness of $N = 103$ parcellated[gif ref] cortical regions was computed[ants ref]; correspondences between cortical region indices and anatomical names are given in Figure 2. An association matrix, or network, A, was generated using correlations in cortical thickness (Figure 3a).

Subnetworks defined using PNA, S_{pna}^j, were generated such that $|Q_{ij}| > 0$, with $i = \{1, ..., N\}$ and $j = \{1,2,3\}$, at 5% significance level, as determined from 1000 bootstrapped samples of A with replacement. Nodes were ranked according to loading magnitude.

For the rich club subnetwork, S_{rc}, normalised weighted rich club coefficients $\varphi_{norm}(k)$[rc ref] were generated over the degree range $1 < k < k_{max}$, where k_{max} was the maximum nodal degree in A. Normalisation was performed using the rich club coefficient averaged over 1000 randomly generated networks[bct ref]. The subnetwork was defined from the nodes that formed the most selective rich club (greatest possible degree threshold) within the rich club regime, defined by the range of k in which $\varphi_{norm}(k) > 1$ and is increasing. Nodes were ranked according to their strength in S_{rc}.

Results: Figures 3b-e and 4a-e display the derived subnetworks. Subnetwork S_{pna}^1 was dominated by nodes with strong positive edges, while nodes with positive and negative edge weights featured in S_{pna}^2, S_{pna}^3 and S_{rc}.

Comparing the nodes in subnetworks S_{pna}^1, S_{pna}^2 and S_{pna}^3 with S_{rc} we find that: 71% of S_{pna}^1 nodes featured in S_{rc}; 100% of S_{pna}^2 nodes featured in S_{rc}; 17% of S_{pna}^3 nodes featured in S_{rc}. Of the 43 nodes in subnetworks S_{pna}^1, S_{pna}^2 and S_{pna}^3 combined, there was 60% agreement with the highest ranked 43 nodes in S_{rc} (Figure 5).

Discussion: Several nodes common to S_{rc} and S_{pna}^1, such as the precuneus, angular gyrus and temporal gyri, correspond to core regions of the default mode network (DMN), which is a highly interconnected area likely to contain hub nodes[ref] with similar connectivity properties. Nodes unique to individual subnetworks were defined by the analysis technique: nodes similarly connected by strong positive correlations were retained in S_{pna}^1, while in S_{rc} positive and negative correlations were retained because both can feature in hub nodes. The primarily anti-correlated nodes in S_{rc} notably appeared in the lower order PNs S_{pna}^2 and S_{pna}^3, reflecting the characteristic property of PNA to group together nodes with similar connectivity attributes.

A limitation on the generation of subnetworks using either technique was their inherent dependency on the inclusion criteria for salient nodes. Bootstrapping the association matrix in PNA provided a more statistically robust set of nodes compared to the simple threshold proposed in the original method[ref]. The degree threshold applied in rich club analysis affected the subnetwork size and therefore the featured anatomical regions; future studies could evaluate subnetworks generated over a range of degree thresholds within the rich club regime.

Conclusions: Subnetworks created using two unrelated techniques for identifying nodes influential in overall network characteristics shared 60% of their 43 highest ranked nodes, several of which belong to the DMN. This suggests that there is a core subset of nodes that are important independently of how "importance" is modelled. The remaining nodes unique to each subnetwork ultimately depend on the biophysical meaning of the analysis technique.

Imaging parameters	
TE (ms)	3.1
TR (ms)	6.9
TI (ms)	824
Resolution (mm3)	1x1x1

Philips Achieva 3T MR scanner;
32-channel head coil

Figure 1: MR acquisition parameters.

Region	Index (right)	Index (left)
cerebellum exterior	1	2
cerebellar vermal lobules I-V	3	3
cerebellar vermal lobules VI-VII	4	4
cerebellar vermal lobules VIII-X	5	5
anterior cingulate gyrus	6	7
anterior insula	8	9
anterior orbital gyrus	10	11
angular gyrus	12	13
calcarine cortex	14	15
central operculum	16	17
cuneus	18	19
entorhinal area	20	21
frontal operculum	22	23
frontal pole	24	25
fusiform gyrus	26	27
gyrus rectus	28	29
inferior occipital gyrus	30	31
inferior temporal gyrus	32	33
lingual gyrus	34	35
lateral orbital gyrus	36	37
middle cingulate gyrus	38	39
medial frontal cortex	40	41
middle frontal gyrus	42	43
middle occipital gyrus	44	45
medial orbital gyrus	46	47
postcentral gyrus medial segment	48	49
precentral gyrus medial segment	50	51
superior frontal gyrus medial segment	52	53
middle temporal gyrus	54	55
occipital pole	56	57
occipital fusiform gyrus	58	59
opercular part of the inferior frontal gyrus	60	61
orbital part of the inferior frontal gyrus	62	63
posterior cingulate gyrus	64	65
precuneus	66	67
parahippocampal gyrus	68	69
posterior insula	70	71
parietal operculum	72	73
postcentral gyrus	74	75
posterior orbital gyrus	76	77
planum polare	78	79
precentral gyrus	80	81
planum temporale	82	83
subcallosal area	84	85
superior frontal gyrus	86	87
supplementary motor cortex	88	89
supramarginal gyrus	90	91
superior occipital gyrus	92	93
superior parietal lobule	94	95
superior temporal gyrus	96	97
temporal pole	98	99
triangular part of the inferior frontal gyrus	100	101
transverse temporal gyrus	102	103

Figure 2: Correspondences between node indices and brain regions.
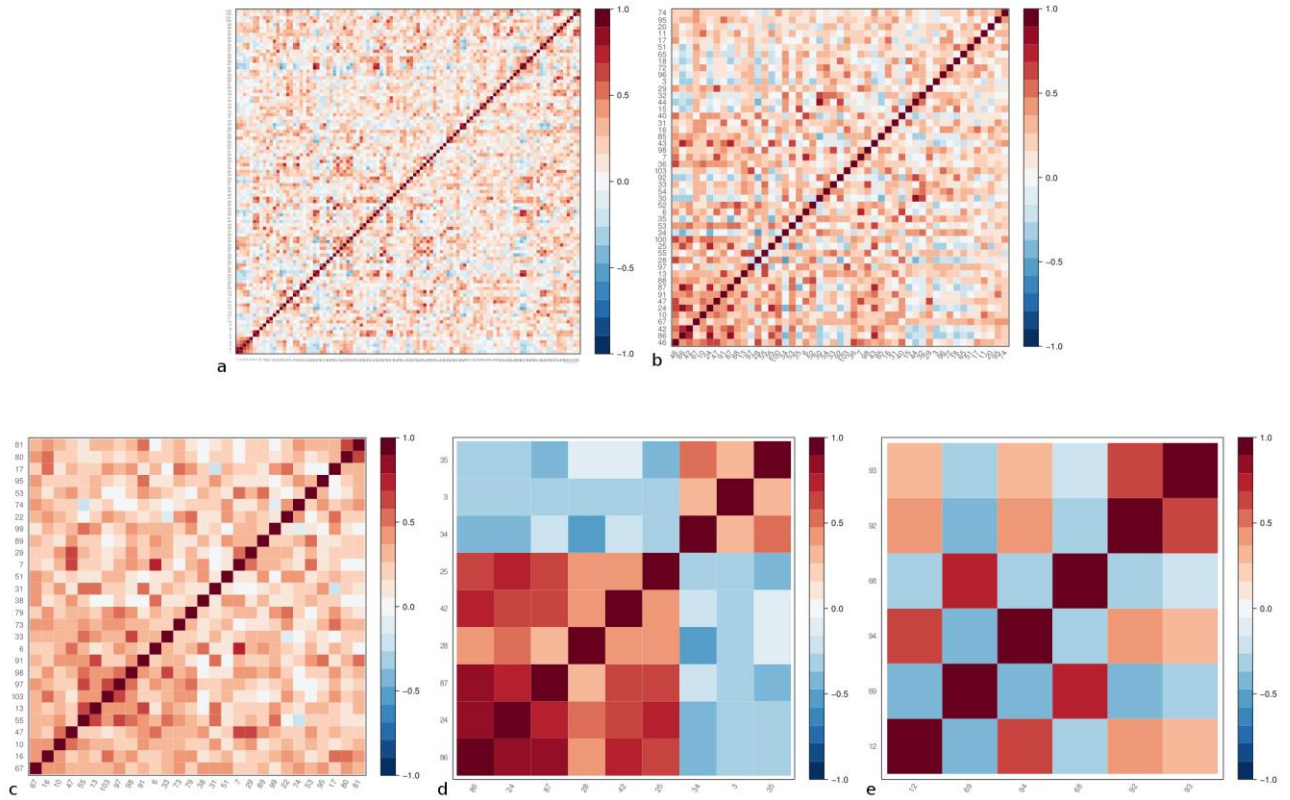
Figure 3: Matrix visualisations of the networks and subnetworks; the colourbar represents Pearson's correlation coefficient between nodes. Nodes in subnetworks b-d are ranked, with the most "important" bottom left. **a)**. Full association network A, containing 103 parcellated cortical regions; **b)**. Subnetwork S_{rc}, with 47 nodes; **c)**. Subnetwork S_{pna}^1, with 28 nodes; **d)**. Subnetwork S_{pna}^2, 9 nodes; **e)**. Subnetwork S_{pna}^3, 6 nodes. Subnetwork S_{pna}^1 is dominated by strong positive connections; subnetworks S_{pna}^2 and S_{rc} contain both positively and negatively correlated nodes.
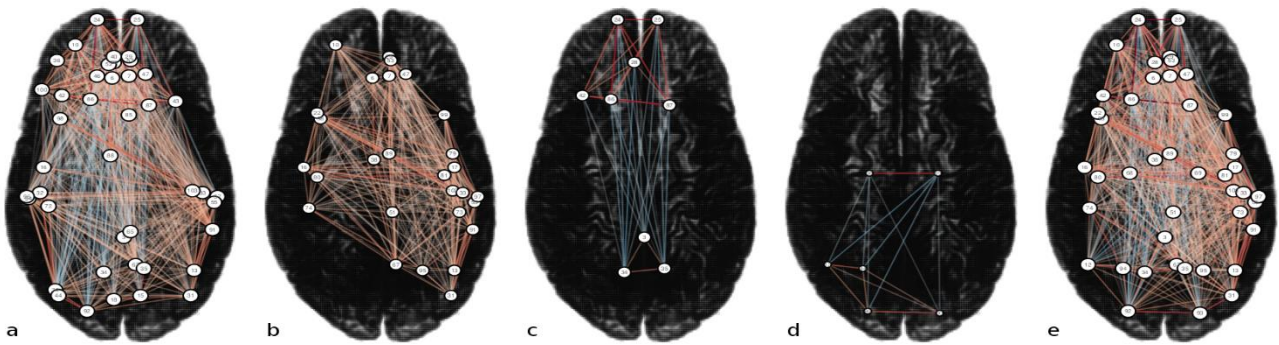
Figure 4: Graphical representation of nodes in each subnetwork. Edge colours represent Pearson's correlation coefficient between nodes: deep red (blue) edges denote strong positive (negative) correlations. Image orientation follows the radiological convention: (image top left is brain anterior right). **a)**. Subnetwork S_{rc}, highest ranked 43 nodes; **b)**. Subnetwork S_{pna}^1; **c)**. Subnetwork S_{pna}^2; **d)**. Subnetwork S_{pna}^3; **e)**. Combined subnetworks S_{pna}^1, S_{pna}^2 and S_{pna}^2, 43 nodes.

Region name	Index (right)	Index (left)
anterior cingulate gyrus	6	7
anterior orbital gyrus	10	
angular gyrus		13
central operculum	16	
gyrus rectus		29
inferior occipital gyrus		31
inferior temporal gyrus		33
medial orbital gyrus		47
superior frontal gyrus medial segment		53
middle temporal gyrus		55
precuneus		67
supramarginal gyrus		91
superior temporal gyrus		97
temporal pole	98	
transverse temporal gyrus		103
cerebellar vermal lobules I V	3	3
frontal pole	24	25
gyrus rectus	28	
lingual gyrus	34	35
middle frontal gyrus	42	
superior frontal gyrus	86	87
superior occipital gyrus	92	

Figure 5: Anatomical regions common to S_{pna}^1 and S_{rc} (top set), to S_{pna}^2 and S_{rc} (middle set), and to S_{pna}^3 and S_{rc} (bottom set). It is interesting to note the laterality of the common regions, particularly between S_{pna}^1 and S_{rc}. It is possible that this is explained in part by the PNA identifying regions in the dominant hemisphere of the primarily right-handed cohort.